Inorganica Chimica Acta 366 (2011) 275–282

Contents lists available at ScienceDirect

Inorganica Chimica Acta

journal homepage: www.elsevier.com/locate/ica

Synthesis, crystal structure, magnetic and redox properties of copper(II) complexes of N-alkyl(aryl) *tBu*-salicylaldimines

Elham Safaei [a,*], Masoume Mohseni Kabir [a], Andrzej Wojtczak [b], Zvonko Jagličić [c], Anna Kozakiewicz [b], Yong-Ill Lee [d]

[a] Institute for Advanced Studies in Basic Sciences (IASBS), 45195 Zanjan, Iran
[b] Nicolaus Copernicus University, Department of Chemistry, 87-100 Torun, Poland
[c] Institute of Mathematics, Physics and Mechanics and Faculty of Civil and Geodetic Engineering, University of Ljubljana, Jadranska 19, SI-1000 Ljubljana, Slovenia
[d] Department of Chemistry, Changwon National University, Changwon 641-773, South Korea

ARTICLE INFO

Article history:
Received 9 September 2010
Received in revised form 6 November 2010
Accepted 10 November 2010
Available online 20 November 2010

Keywords:
Copper complexes
Phenoxyl
Enzyme models
5-Bu$^t_2$-salicylaldimine
3,5-Bu$^t_2$-salicylaldimine

ABSTRACT

A series of novel copper(II) complexes, L_2Cu with newly synthesized 3,5-Bu$^t_2$-salicylaldimine (or 5-Bu$^t_2$-salicylaldimine) ligands derived from 2,4-di-tert-butyl phenol (or 4-tert-butyl phenol) and alkyl (aryl) amines have been prepared and their spectroscopic (IR, UV–Vis, ESI-MS), X-ray, magnetic and redox properties have been investigated. The X-ray crystallography analysis shows that all complexes are monomeric and their copper(II) centers are surrounded by phenolate oxygens and imine nitrogen atoms. Therefore, the coordination sphere around the copper atoms is N_2O_2 as seen in galactose oxidase active site. In addition, the geometric configurations of all complexes are square planar or slightly distorted square planar. The crystal system for all complexes is monoclinic, except for L^1_2Cu which is orthorhombic. The temperature dependence of magnetic susceptibility of complexes confirms the mononuclear structure of complexes. Oxidation of the Cu(II) complexes yielded the corresponding Cu(II)-phenoxyl radical species during the cyclic voltammetry experiments.

1. Introduction

Metalloenzymes control a wide range of functions in the biological systems. Galactose oxidases (GOA), cytochrome c oxidase (Cco), iron-containing ribonucleotide reductase (RR) are typical examples of these enzymes [1–4]. Galactose oxidase (GOA) is an enzyme containing single Cu ion (Scheme 1) which belongs to the family of oxidoreductases. It contains a cysteine-modified phenol moiety of Tyr 272 (Y_{272}) and a phenol group of tyrosine 495 (Y_{495}) coordinated to a copper(II) center. This enzyme catalyzes the oxidation of D-galactose and wide range of primary alcohols with concomitant reduction of dioxygen to hydrogen peroxide [5–22].

The proposed mechanism (Scheme 2) of oxidation by GOase involves a cycle of the three distinct oxidation states: the fully oxidized form (Cu^{2+}-Tyr$^{\cdot}$), fully reduced form (Cu^{+}-Tyr) and semi form (Cu^{2+}-Tyr) which is catalytically inactive [22].

Extensive efforts have been made to provide a valuable insight into the structure and reactivity of GOA active site. Salen and tripodal ligands have been widely employed to provide a coordination sphere as models for the active site of this enzyme. Several research groups have synthesized the biomimetic model complexes with O,N,O coordination sphere (usually amine nitrogen and phenolic oxygen atoms) [23–27].

We focused our interest on copper complexes of iminophenolate ligands involving easily oxidizable bulky 3,5-Bu$^t_2$-phenols producing more stable phenoxyl radical complexes due to their structural similarities to galactose oxidase active site. In the present work, we have synthesized several N-alkyl (aryl) salicylaldimine ligands, H_2L, with O and N donor atoms bearing alkyl or aryl groups and their copper(II) complexes (Scheme 3). The coordination, magnetic and redox properties of these complexes are described.

2. Experimental

2.1. Materials and physical measurements

Reagents or analytical grade materials were obtained from commercial suppliers and used without further purification, except those for electrochemical measurements. 3,5-Bu$^t_2$-salicylaldehyde (3,5-DTBS) and 5-Bu$^t_2$-salicylaldehyde (5-TBS) were prepared by the literature method [28,29].

Elemental analyses (C. H. N.) were performed by the Research Institute of Petroleum Industry (RIPI). Fourier transform infrared

* Corresponding author. Tel.: +98 241 4153200; fax: +98 241 4153232.
E-mail address: safaei@iasbs.ac.ir (E. Safaei).

0020-1693/$ - see front matter © 2010 Elsevier B.V. All rights reserved.
doi:10.1016/j.ica.2010.11.017

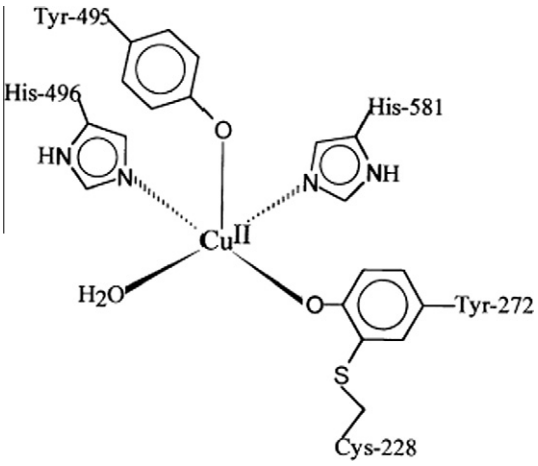

Scheme 1. Structure of the GOA catalytic center [22].

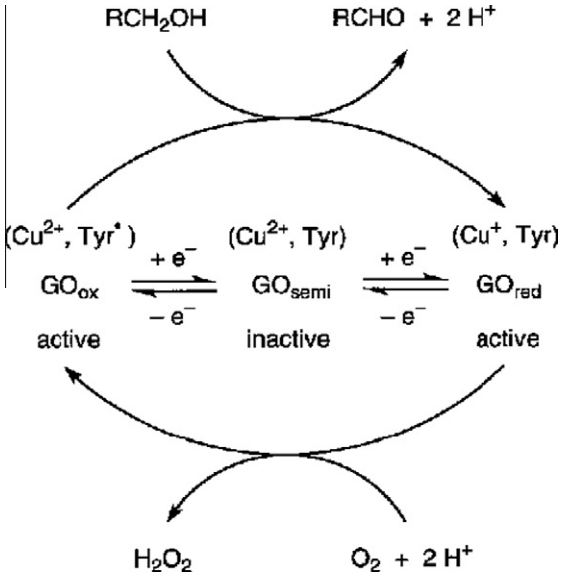

Scheme 2. Redox states of GAO [22].

spectroscopy on KBr pellets was performed on a FT IR Bruker Vector 22 instrument. NMR measurements were performed on a Bruker 250 instrument. UV–Vis absorbance digitized spectra were collected using a CARY 100 spectrophotometer. The electronic spectra of all complexes recorded in CH_3CN.

The ligand samples were dissolved in acetonitrile (1.0×10^{-4} M) and mixed with deionized water (1:1) just before the mass spectroscopic measurements. The identification of interaction products was performed using Thermo Finigan LCQ Advantage ion trap mass spectrometer equipped with electrospray ionization. For sample injections, the instrument syringe pump was used at flow rate of 2 L/min. The instrumental operation conditions were as follows; spray voltage, 4.58 kV; source current, 0.48 A; sheath gas flow rate, 19.43 L/min; capillary voltage; 9.44 V, capillary temperature 100 °C, tube lens voltage; 55 V. Experiments were performed in positive-ion mode and optimized by Xcalibur software before the experiments. All MS experiments in this work have been carried out under the optimized instrument conditions. All reported mass spectra are the average of at least 30 consecutive scans.

Magnetic susceptibility were measured from powder samples of solid material in the temperature range 2–300 K by using a

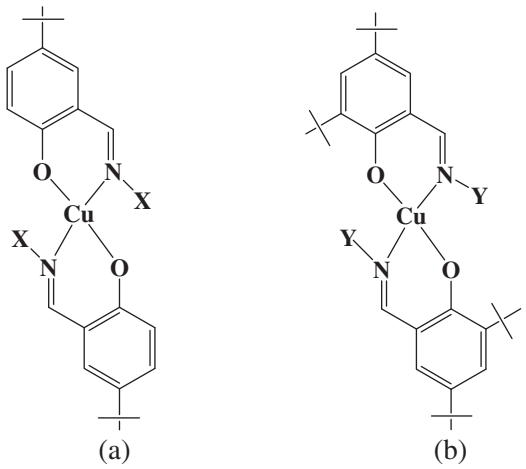

Ligand	(**X**)
HL^1	$-CH_3$
HL^2	$-(CH_2)_3CH_3$
HL^3	$-CH_2C_6H_5$
HL^4	$-C_6H_5$
HL^5	$-C_6H_5OCH_3$
HL^6	$-C_{10}H_7$
Ligand	(**Y**)
HL'^1	$-CH_3$
HL'^2	$-(CH_2)_3CH_3$

Scheme 3. The structure of bis(N-Y-5-Bu^t_2-salicylaldiminate) copper complex (a) and bis(N-X- 3,5-Bu^t_2-salicylaldiminate) copper complex (b).

SQUID susceptometer (Quantum Design MPMS-XL-5) in a magnetic field of 1000 Oe.

Voltammetric measurements were made with a computer controlled Auto Lab electrochemical system (ECO Chemie, Ultrecht, The Netherlands) equipped with a PGSTA 30 model and driven by GPES (ECO Chemie). A glassy carbon electrode with a surface area of 0.035 cm^2 was used as a working electrode and a platinum wire served as the counter electrode. The reference electrode was an Ag wire as the quasi reference electrode. Ferrocene was added as an internal standard after completion of a set of experiments, and potentials are referenced vs. the ferrocenium/ferrocene couple (Fc^+/Fc).

The X-ray data for the reported complexes were collected with an Oxford Sapphire CCD diffractometer using Mo Kα radiation $\lambda = 0.71073$ Å, at 293(2) or 292(2) K, by ω-2θ method. Structures have been solved by direct methods and refined with the full-matrix least-squares method on F^2 with the use of SHELX97 [30] program package. The numerical absorption correction was applied (RED171 package of programs [31] Oxford Diffraction, 2000). No extinction correction was applied. Positions of hydrogen atom have been found from the electron density maps, and hydrogen atoms were constrained in the refinement.

2.2. Preparations

2.2.1. Synthesis of ligands

All salicylaldimines *HL*, N-(1-methyl)-5-Bu^t_2-salicylaldimine, N-(1-butyl)-5-Bu^t_2-salicylaldimine, N-(1-benzyl)-5-Bu^t_2-salicylaldimine, N-(1-phenyl)-5-Bu^t_2-salicylaldimine, N-(1-methoxy-phenyl)-5-Bu^t_2-salicylaldimine, N-(1-naphthyl)-5-Bu^t_2-salicylaldimine,

and HL′, N-(1-methyl)-3,5-Bu^t_2-salicylaldimine, N-(1-butyl)-3,5-Bu^t_2-salicylaldimine were prepared with good yields via condensation of the 3,5-Bu^t_2-salicylaldehyde (3,5-DTBS) or 5-Bu^t_2-salicylaldehyde (5-TBS) with the corresponding amines (1:1 M ratio) in methanol at 50 °C for 5 h.

2.2.1.1. Synthesis of ligands HL. A solution of 5-Bu^t_2-salicylaldehyde (1 mmol, 0.17 g) and amine (1 mmol) in 5 ml methanol was stirred for 3 h at 50 °C. After cooling, obtained yellow product was filtered and re-crystallized from dichloromethane/methanol (2:1). The solution remaining after the removal of the solid was left to give more products.

2.2.1.1.1. Ligand HL^1. (20.15% yield). ^{1}H NMR ($CDCl_3$): δ 13.232 (s, 1H), 8.345 (s, 1H), 7.325 (m, 3H), 3.746 (s, 3H), 1.292 (s, 9H). IR(KBr, cm^{-1}): 3424w, 2958s, 1638s, 1491 m, 1399 m, 1266s, 1109w, 1019w, 827s.

2.2.1.1.2. Ligand HL^2. (18.02% yield). M.P. 100.7, ^{1}H NMR ($CDCl_3$): δ 13.998 (s, 1H), 8.356 (s, 1H), 7.221(m, 3H), 3.588 (s, 3H), 2.596 (s, 4H), 2.316 (s, 2H) 1.289 (s, 9H). IR(KBr, cm^{-1}): 3432s, 2957 m, 2362w, 1623s, 1587sh, 1489s, 1365w, 1264 m, 1178 m, 818 m, 694w. m.p. 100.7.

2.2.1.1.3. Ligand HL^3. (82.77% yield). M.P. 102.4, ^{1}H NMR ($CDCl_3$): δ 13.195 (s, 1H), 8.466 (s, 1H), 7.344 (m, 8H), 4.827 (s, 2H), 1.323 (s, 9H). IR(KBr, cm^{-1}): 3428w, 3024s, 2957sh, 1631s, 1583sh, 1487s, 1445sh, 1372sh, 1261 m, 1181 m, 1124sh, 1054sh, 964w, 924sh, 886sh, 828sh, 728sh, 704sh, 657sh, 621sh, 453sh. m.p. 102.4.

2.2.1.1.4. Ligand HL^4. (20.75% yield). M.P. 96.9, ^{1}H NMR ($CDCl_3$): δ 13.040 (s, 1H), 8.649 (s, 1H), 7.282 (m, 8H), 1.361(s, 9H). IR(KBr, cm^{-1}): 3429w, 2957 m, 2354 m, 1619s, 1575sh, 1490s, 1359w, 1258 m, 1178s, 1138sh, 1027w, 982w, 927w, 889w, 823s, 696 m, 650w, 621w. m.p. 96.9.

2.2.1.1.5. Ligand HL^5. (14.13% yield). M.P. 98.7, ^{1}H NMR ($CDCl_3$): δ 13.209 (s, 1H), 8.633 (s, 1H), 7.252 (m, 7H), 3.848 (s, 3H), 1.328 (s, 9H). IR(KBr, cm^{-1}): 3430 m, 2956s, 2544w, 2049w, 1620s, 1498s, 1362w, 1293sh, 1252s, 1180 m, 1110w, 1031 m, 965w, 828s, 531 m. m.p. 98.7.

2.2.1.1.6. Ligand HL^6. (38.11% yield). M.P. 115.1, ^{1}H NMR ($CDCl_3$): δ 13.037 (s, 1H), 8.736 (s, 1H), 7.557 (m, 10H), 1.353 (s, 9H). IR(KBr, cm^{-1}): 3420w, 3047w, 2955s, 2866sh, 1617s, 1566sh, 1488s, 1450sh, 1388s, 1257s, 1192sh, 1081w, 1031w, 971w, 937w, 882 m, 819sh, 775s, 650w, 623w, 579w. m.p. 115.1.

2.2.1.2. Synthesis of ligands HL′. In a round bottom flask, a solution of 3,5-Bu^t_2-salicylaldehyde (1 mmol, 0.234 g) and amine (1 mmol) in 5 ml methanol was stirred for 5 h at 50 °C. After cooling, obtained yellow product was filtered and re-crystallized from dichloromethane/ethanol (2:1).

2.2.1.2.1. Ligand HL'^1. (38.25% yield). ^{1}H NMR ($CDCl_3$): δ 13.020 (s, 1H), 8.349 (s, 1H), 7.263 (m, 2H), 3.760 (s, 3H), 1.564 (s, 9H), 1.658 (s, 9H). IR(KBr, cm^{-1}): 3439s, 2896sh, 2779w, 1639s, 1493s, 1400 m, 1365sh, 1263s, 1188w, 1134w, 1017 m, 965w, 927w, 878w, 828s, 716w, 655w, 616w, 484w.

2.2.1.2.2. Ligand HL'^2. (59.86% yield). ^{1}H NMR ($CDCl_3$): δ 14.002 (s, 1H), 8.346 (s, 1H), 7.216 (m, 2H), 3.596 (s, 3H), 2.583 (s, 4H), 2.321 (s, 2H), 1.563 (s, 9H), 1.659 (s, 9H). IR(KBr, cm^{-1}): 3422w, 2959s, 1632s, 1470s, 1367 m, 1241 m, 1173sh, 1121w, 1025w, 941 m, 870w, 815w, 737w, 648w, 602w, 455 m.

2.2.2. Synthesis of complexes

2.2.2.1. Synthesis of complexes L_2Cu. To the solution of synthesized imines (HL) (1 mmol), dry triethylamine (1 mmol, 0.138 ml) and copper acetate monohydrate (1 mmol, 0.199 g) was added and the mixture was stirred for 2 h in reflux conditions. Then the brown solution was obtained, filtered and re-crystallized from dichloromethane:methanol (2:1) and in one instance from dichloromethane:ethanol (2:1).

2.2.2.1.1. Complex L^1_2Cu. (15.57% yield). *Anal.* Calc. for $C_{24}H_{32}CuN_2O_2$ (443.19 g/mol): C, 64.9; H, 7.2; N, 6.3. Found: C, 66.2; H, 8.4; N, 7%. IR(KBr, cm^{-1}): 3450w, 2956s, 1628s, 1535 m, 1484sh, 1417 m, 1374 m, 1326 m, 1258 m, 1182w, 1098w, 1021w, 873s, 828sh, 715w, 604w, 529w, 457w. ESI MS: m/z = 443.

2.2.2.1.2. Complex L^2_2Cu. (53.13% yield). *Anal.* Calc. for $C_{30}H_{44}CuN_2O_2$ (527.28.19 g/mol): C, 68.2; H, 8.4; N, 5.3. Found: C, 69.1; H, 8.6; N, 5.5%. IR(KBr, cm^{-1}): 3452w, 2956s, 2863sh, 1625s, 1532sh, 1479s, 1388sh, 1328 m, 1257 m, 1214 m, 1177 m, 1140w, 1028w, 880s, 829sh, 720w, 605w, 514w, 454w. ESI MS: m/z = 527.

2.2.2.1.3. Complex L^2_3Cu. (31.93% yield). *Anal.* Calc. for $C_{36}H_{40}CuN_2O_2$ (595.25 g/mol): C, 72.6; H, 6.3; N, 4.7. Found: C, 71.2; H, 6.9; N, 4.4%. IR(KBr, cm^{-1}): 2955s, 2914sh, 2864sh, 1616s, 1531 m, 1464s, 1388 m, 1322s, 1257 m, 1173 m, 1141w, 1102w, 1015 m, 890s, 826sh, 747 m, 688 m, 614 m, 584sh, 487 m. ESI MS: m/z = 595.

2.2.2.1.4. Complex L^4_2Cu. (55.20% yield). *Anal.* Calc. for $C_{34}H_{38}CuN_2O_2$ (567.22 g/mol): C, 71.6; H, 6.7; N, 4.9. Found: C, 72.8; H, 6.6; N, 5.1%. IR(KBr, cm^{-1}): 3447w, 3018s, 2953sh, 1615s, 1585sh, 1523 m, 1468s, 1413 m, 1374 m, 1324 m, 1258 m, 1170s, 1019w, 877 m, 832sh, 754 m, 701 m, 606w, 531 m, 446w. ESI MS: m/z = 567.

2.2.2.1.5. Complex L^5_2Cu. (32.85% yield). *Anal.* Calc. for $C_{36}H_{42}CuN_2O_2$ (627.24 g/mol): C, 68.8; H, 6.7; N, 4.4. Found: C, 67.6; H, 6.3; N, 4.5%. IR(KBr, cm^{-1}): 3430w, 3005s, 2954sh, 2359w, 1616s, 1511sh, 1463s, 1376 m, 1315 m, 1253s, 1168s, 1107sh, 1026 m, 1021w, 882s, 828sh, 688w, 600 m, 526w. ESI MS: m/z = 627.

2.2.2.1.6. Complex L^6_2Cu. (24.59% yield). *Anal.* Calc. for $C_{42}H_{42}CuN_2O_2$ (667.25 g/mol): C, 75.5; H, 5.3; N, 4.1. Found: C, 74.9; H, 6.2; N, 3.7%. IR(KBr, cm^{-1}): 3446w, 3052s, 2955sh, 1605s, 1525 m, 1467s, 1382 m, 1325 m, 1257 m, 1175 m, 1085w, 1028w, 831 m, 778 ms, 694w, 550w, 508w. ESI MS: m/z = 681.

2.2.2.2. Synthesis of complexes $L_2'Cu$. To the solution of synthesized imines (HL′) (1 mmol), dry triethylamine (1 mmol, 0.138 ml) and copper acetate monohydrate (1 mmol, 0.199 g) was added and the mixture was stirred for 2 h in room temperature. Then the brown solution was obtained, filtered and re-crystallized from dichloromethane:methanol (2:1).

2.2.2.2.1. Complex L'^1_2Cu. (16.39% yield). *Anal.* Calc. for $C_{32}H_{48}CuN_2O_2$ (555.31 g/mol): C, 71.3; H, 9.3; N, 4.4. Found: C, 68.6; H, 8.6; N, 5.5%. IR(KBr, cm^{-1}): 3421w, 2955s, 1627s, 1537 m, 1428s, 1353sh, 1316 m, 1262 m, 1166 m, 1098w, 1027 m, 914 m, 870 m, 829w, 795sh, 740 m, 635 m, 536sh, 461 m. ESI MS: m/z = 556.

2.2.2.2.2. Complex L'^2_2Cu. (31.14% yield). *Anal.* Calc. for $C_{38}H_{60}CuN_2O_2$ (639.41 g/mol): C, 71.2; H, 9.4; N, 4.3. Found: C, 71.5; H, 9.3; N, 4.4%. IR(KBr, cm^{-1}): 3447w, 2957s, 1622s, 1536 m, 1444 m, 1398sh, 1317w, 1261 m, 1167w, 1116w, 1028w, 873w, 797w, 744w, 538w. ESI MS: m/z = 639.

3. Results and discussion

All salicylaldimines ligands, HL, were synthesized from 3,5-Bu^t_2-salicylaldehyde (3,5-DTBS) or 5-Bu^t_2-salicylaldehyde (5-TBS) with the corresponding amines in a single-step condensation.

The ligands HL or HL′ in methanol were treated with copper acetate, triethylamine in suitable ratio and the solution was refluxed to yield L_2Cu and L'_2Cu complexes, with relatively high yields.

In IR spectra of all ligands (HL), ν_{OH} stretch is observed in the range 2900–3000 cm^{-1}. The occurrence of this band at such a relatively low wave number is characteristic of these ligands and is an indication of extensive hydrogen bonding. The ν(C=N) band in the spectra of the free ligands is observed in the region

1620–1640 cm^{-1}. In IR spectra of the complexes, the strong and sharp band at frequencies around 3000 cm^{-1} for the ν_{OH} stretch of ligands disappeared, proving the coordination of phenol groups to the metal. The ν(C=N) band in the complexes IR spectra shifted to lower frequencies 1600–1630 cm^{-1}, what indicates coordination of the azomethine nitrogen to the metal.

The electronic spectra of all complexes recorded in CH_2Cl_2 are presented in Sections 2.2.2.1 and 2.2.2.2. The intra-ligand absorptions <400 nm are assigned to π–π* and n–π* transitions. The higher energy transition is assigned to a phenolate-to-Cu(II) charge transfer transition, on the basis of comparisons with the UV/Vis spectra of other Cu(II)-phenolate complexes. The bands observed around 650 nm are assigned to d–d transitions.

The ESI-MS spectrum gave a relatively weak ML_2H^+ ion peaks, a proton attached molecule, what clearly indicated the formation of 2:1 complexes, and intense peaks related to protonated ligands $(L + H)^+$. The original spectrum is shown in Supplementary material. The molecular peaks of the complex ions are shown in Sections 2.2.2.1 and 2.2.2.2.

3.1. X-ray Data collection and structure determination of L_2Cu and L'_2Cu

Crystal data for the investigated complexes are tabulated in Table 1. The selected bond lengths and angles are presented in Table 2.

Table 1
Crystal data for complex structures L^1_2Cu, L^2_3Cu, L^5_2Cu, L^6_2Cu and L'^1_2Cu.

	L^1_2Cu	L^2_3C	L^5_2Cu	L^6_2Cu	L'^1_2Cu
Empirical formula	$C_{24}H_{32}CuN_2O_2$	$C_{36}H_{40}CuN_2O_2$	$C_{36}H_{40}CuN_2O_4$	$C_{42}H_{40}CuN_2O_2$	$C_{32}H_{48}CuN_2O_2$
Formula weight	444.06	596.24	628.24	668.3	556.26
Temperature (K)	293(2)	293(2)	292(2)	292(2)	293(2)
Wavelength (Å)	0.71073	0.71073	0.71073	0.71073 Å	0.71073
Crystal system	orthorhombic	monoclinic	monoclinic	monoclinic	monoclinic
Space group	Pbcm	P2(1)/c	P2(1)/c	P2(1)/c	P2(1)/n
Unit cell dimensions (Å)	a = 18.031 (4)	a = 12.4516 (10)	a = 17.9630 (4)	a = 12.4325 (17)	a = 13.823 (3)
	b = 19.315 (4)	b = 5.9692 (5)	b = 6.98550 (10)	b = 7.1542 (13)	b = 17.846 (4)
	c = 6.6500 (10)	c = 20.5661 (17)	c = 26.4128 (7)	c = 19.891 (4)	c = 13.031 (3)
	–	β = 90.349 (7)	β = 90.091 (2)	β = 104.062 (14)	β = 102.05 (3)
Volume (Å^3)	2316.0 (8)	1528.6 (2)	3314.29 (12)	1716.2 (5)	3143.7 (12)
Z, density (calc.) (Mg/m^3)	4, 1.274	2, 1.295	4, 1.259	2, 1.293	4, 1.175
Absorption coeff. (mm^{-1})	0.964	0.749	0.699	0.675	0.723
Maximum and minimum transmission	0.8934 and 0.6243	0.8528 and 0.7823	0.8975 and 0.7205	0.9072 and 0.7025	0.9457 and 0.6436
F(0 0 0)	940	630	1324	702	1196
Crystal size (mm)	0.54 × 0.23 × 0.12	0.34 × 0.23 × 0.22	0.50 × 0.32 × 0.16	0.56 × 0.24 × 0.15	0.67 × 0.63 × 0.08
θ Range for data collect (°)	2.11–26.00	2.56–31.18	2.27–28.57	2.36–26.00	2.26–31.35
Limiting indices	$-22 \geqslant h \leqslant 22$	$-17 \geqslant h \leqslant 18$	$-23 \geqslant h \leqslant 22$	$-15 \geqslant h \leqslant 15$	$-20 \geqslant h \leqslant 19$
	$-23 \geqslant k \leqslant 23$	$-7 \geqslant k \leqslant 8$	$-9 \geqslant k \leqslant 9$	$-6 \geqslant k \leqslant 8$	$-24 \geqslant k \leqslant 25$
	$-7 \geqslant l \leqslant 8$	$26 \geqslant l \leqslant 29$	$-35 \geqslant l \leqslant 33$	$-24 \geqslant l \leqslant 24$	$-14 \geqslant l \leqslant 18$
Reflected collected	14 438	14 478	33 424	12 105	30 796
Independent reflect	2949; R(int) = 0.0334	4656; R(int) = 0.0329	7746; R(int) = 0.0273	3366; R(int) = 0.139	9595; R(int) = 0.0850
Completeness	99.90%	99.80%	99.90%	99.80%	99.90%
Data/restraints/param.	2490/0/181	4656/0/190	7746/0/388	3366 0/214	9595/18 3
Goodness-of-fit (GOF)on F^2	1.207	1.11	1.054	1.2095	1.028
Final R indices [$I > 2\sigma(I)$]	R_1 = 0.0541,	R_1 = 0.0398,	R_1 = 0.0384,	R_1 = 0.0710,	R_1 = 0.0566,
	wR_2 = 0.1391	wR_2 = 0.0998	wR_2 = 0.1076	wR_2 = 0.1797	wR_2 = 0.1414
R indices (all data)	R_1 = 0.0661,	R_1 = 0.0570,	R_1 = 0.0557,	R_1 = 0.0854,	R_1 = 0.0999,
	wR_2 = 0.1432	wR_2 = 0.1073	wR_2 = 0.1132	wR_2 = 0.1937	wR_2 = 0.1647
Largest difference in peak and hole (e Å^{-3})	0.466 and −0.945	0.330 and −0.299	0.730 and −0.294	0.382 and −0.742	0.559 and −0.465

Table 2
Selected bond lengths (Å) and angles (°) for complex structures L^1_2Cu, L^2_3Cu, L^5_2Cu, L^6_2Cu and L'^1_2Cu.

L^1_2Cu	L^1_2Cu	L^2_3Cu	L^2_3Cu	L^5_2Cu	L^5_2Cu	L^6_2Cu	L^6_2Cu	L'^1_2Cu	L'^1_2Cu
Cu1–O21	1.879(3)	Cu1–O1#1	1.8798(12)	Cu1–O21	1.8760(14)	Cu1–O1#1	1.870(3)	Cu1–O2	1.8913(16)
Cu1–O1	1.887(3)	Cu1–O1	1.8798(12)	Cu1–O1	1.8783(13)	Cu1–O1	1.870(3)	Cu1–O1	1.9026(18)
Cu1–N21	1.994(4)	Cu1–N1#1	1.9999(12)	Cu1–N21	1.9664(14)	Cu1–N1#1	1.994(3)	Cu1–N2	1.9442(19)
Cu1–N1	1.9967(4)	Cu1–N1	1.9999(12)	Cu1–N1	1.9758(15)	Cu1–N1	1.994(3)	Cu1–N1	1.9600(19)
O21–Cu1–O1	179.44(14)	O1#1–Cu1–O1	180.00(10)	O21–Cu1–O1	143.95(6)	O1#1–Cu1–O1	180.0	O2–Cu1–O1	156.97(8)
O21–Cu1–N21	91.84(15)	O1#1–Cu1–N1#1	91.68(5)	O21–Cu1–N21	95.72(6)	O1#1–Cu1–N1#1	91.79(12)	O2–Cu1–N2	93.20(8)
O1–Cu1–N21	88.72(15)	O1–Cu1–N1#1	88.32(5)	O1–Cu1–N21	98.11(6)	O1–Cu1–N1#1	88.22(12)	O1–Cu1–N2	92.05(8)
O21–Cu1–N1	87.54(15)	O1#1–Cu1–N1	88.32(5)	O21–Cu1–N1	96.22(6)	O1#1–Cu1–N1	88.22(12)	O2–Cu1–N1	91.19(7)
O1–Cu1–N1	91.90(15)	O1–Cu1–N1	91.68(5)	O1–Cu1–N1	94.40(6)	O1–Cu1–N1	91.79(12)	O1–Cu1–N1	92.00(8)
N21–Cu1–N1	179.38(15)	N1#1–Cu1–N1	180.00(10)	N21–Cu1–N1	139.69(6)	N1#1–Cu1–N1	180.0	N2–Cu1–N1	158.73(9)
C1–O1–Cu1	130.0(3)	C1–O1–Cu1	129.41(11)	C1–O1–Cu1	127.54(12)	C11–O1–Cu1	128.9(2)	C1–O1–Cu1	126.34(15)
C7–N1–Cu1	124.6(3)	C7–N1–Cu1	123.37(10)	C7–N1–Cu1	123.73(13)	C9–N1–Cu1	123.7(3)	C7–N1–Cu1	122.74(16)
C8–N1–Cu1	119.7(3)	C8–N1–Cu1	121.84(10)	C8–N1–Cu1	116.97(11)	C1–N1–Cu1	120.7(2)	C16–N1–Cu1	119.02(16)
C21–O21–Cu1	130.5(3)	C1#1–O1#1–Cu1	129.41(11)	C21–O21–Cu1	126.12(12)	C11#1–O11#1–Cu1	128.9(2)	C21–O2–Cu1	128.54(15)
C27–N21–Cu1	124.2(3)	C7#1–N1#1–Cu1	123.37(10)	C27–N21–Cu1	122.08(12)	C9#1–N1#1–Cu1	123.7(3)	C27–N2–Cu1	123.70(17)
C28–N21–Cu1	120.3(3)	C8#1–N1#1–Cu1	121.84(10)	C28–N21–Cu1	118.24(11)	C1#1–N1#1–Cu1	120.7(2)	C36–N2–Cu1	119.69(17)

Symmetry transformations used to generate equivalent atoms: L^2_3Cu #1 $-x,-y,-z$; L^6_2Cu #1 $-x+1,-y,-z$.

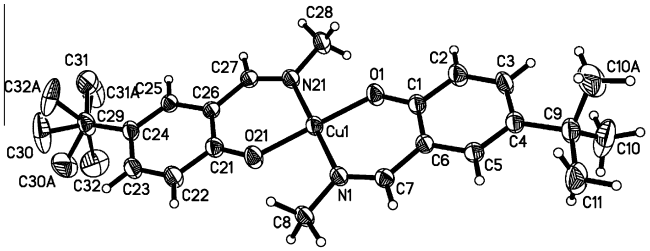

Fig. 1. ORTEP diagram and atom labeling scheme for complex L^1_2Cu. Atoms denoted A are related to the basic set by the mirror plane symmetry transformation [*x*,*y*,1/2−*z*]. Hydrogen atoms in the disordered tert-Bu group are not displayed.

Structure of L^1_2Cu is build up with the complexes molecule positioned on the mirror plane in the Pbcm space group. Consequently, the square-planar coordination sphere has no deformations connected to the donor atom displacement from that plane. The structure analysis revealed the rotational disorder of the tert-Bu group of one ligand, with all methyl groups positioned out of the mirror plane (Fig. 1). That resulted in two populations of that group related by the mirror plane symmetry [*x*,*y*,1/2−*z*], both populated 50%. In the second ligand, one methyl group of tert-Bu is positioned exactly on the mirror plane, while remaining pair is related by the mirror plane. The N-bound C8 and C28 methyl groups in both ligands are also positioned in the mirror plane. Consequently for each of them, one H atom is located on that plane, while two other are related by the mirror plane symmetry. Crystal packing analysis revealed the parallel orientation of the complex molecules. The distance between centers of gravity of the Cu1–O1–C1–C6–C7–N1 chelate ring and its equivalent transformed with [*x*,1/2−*y*,−*z*] is 3.4809(8) Å, while for chelate Cu1–O21–C21–C26–C27–N21 ring and its [*x*,1/2−*y*,−*z*] equivalent it is 3.3529(7) Å. In such orientation of the molecules, there is a short Cu1...Cu1[*x*,1/2−*y*,−*z*] distance of 3.3405(7).

Structure of L^2_3Cu is centrosymmetric, with the Cu(II) positioned on the center of symmetry (Fig. 2). The ligand contains the N-benzyl moiety much larger that the N-methyl present in L^1_2Cu. The steric hindrance between the phenolate in the coordination sphere and the N-bound benzyl moiety is minimized by the rotation around N1–C8 and C8–C9 bonds, with the consecutive torsion angles in the C7–N1–C8–C9–C10 fragment being 88.12(16) and −123.14(17)°. The C6–C7–N1–C8 fragment is planar, with the torsion angle −174.94(15). The phenolic ring and the phenyl ring in the ligand are almost perpendicular to each other, and the dihedral angle between their best planes is 77.53°.

The asymmetric part of structure of L^5_2Cu contains the whole complex molecule (Fig. 3). Replacement of benzyl with phenyl group bound to N atom increases the steric hindrance within the coordination sphere, when compared to L^2_3Cu. The dihedral angle between the phenolic ring and the phenyl ring in the ligand differs significantly for two ligands. It is 50.67° between C1–C6 and C8–C13 and only 25.69° between C21–C26 and C28–C33 rings. That results from different inter-molecular interactions of both phenyl rings. The C8–C13 ring interacts with its equivalent related by [2−*x*,1−*y*,−*z*] transformation, the distance between the centers of gravity being 4.291 Å. Contrary, the C28–C33 ring forms the interaction to the chelate ring Cu1–O21–C21–C26–C27–N21, with the distance between their centers of gravity being 3.824 Å.

The asymmetric part of L^6_2Cu contains a half of the molecule with the Cu positioned on the center of symmetry (Fig. 4). The other part is generated by the center of symmetry with [−*x* + 1, −*y*, −*z*] transformation. The possible steric hindrance caused by the N-naphtyl moiety is decreased by the rotation around the single N1–C1 bond, with the torsion angle C9–N1–C1–C2 of 61.8(5)°. Analysis of crystal packing reveals the C2–H...π interaction with the phenolic C10–C15 ring transformed by [1−*x*,1−*y*,−*z*], the distance between C–H and center of gravity of the ring being 2.78 Å.

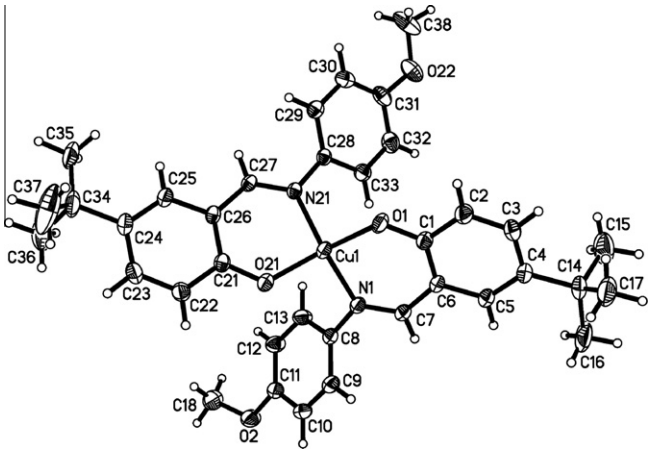

Fig. 3. ORTEP diagram and atom labeling scheme for complex L^5_2Cu.

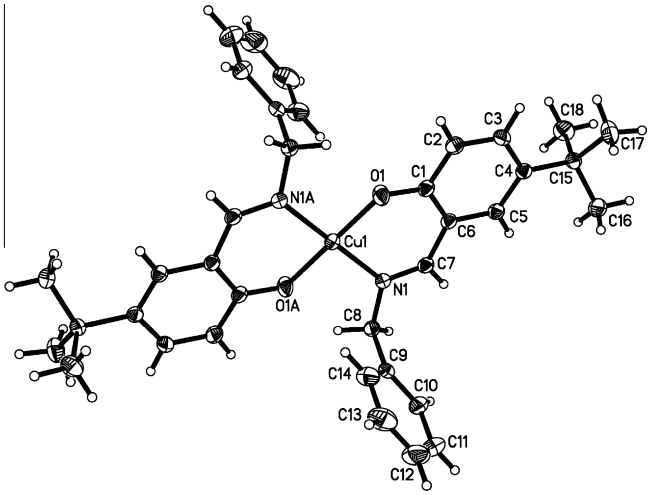

Fig. 2. ORTEP diagram and atom labeling scheme for complex L^2_3Cu. Half of the molecule constitutes the asymmetric part of the structure. Ligand denoted with *A* is generated by the center of symmetry transformation [−*x*, −*y*, −*z*].

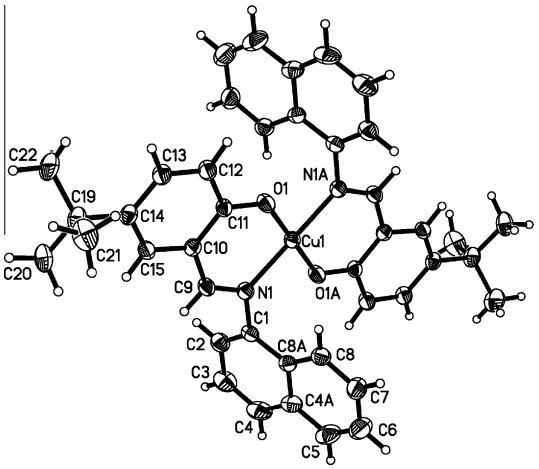

Fig. 4. ORTEP diagram and atom labeling scheme for complex L^6_2Cu. Half of the complex molecule constitutes the asymmetric part of the structure. Ligand denoted with *A* is generated by the center of symmetry transformation [−*x* + 1, −*y*, −*z*].

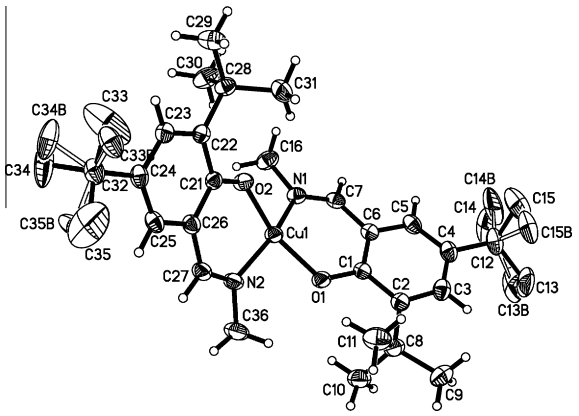

Fig. 5. ORTEP diagram and atom labeling scheme for complex $L_1'^2Cu$. Hydrogen atoms of the disordered tert-Bu groups are omitted for clarity.

In the $L_2'^1Cu$ structure the whole complex molecule constitutes the asymmetric part of the structure (Fig. 5). Two tert-Bu substituents in the phenolic ring reveal different rotational flexibility, depending on their position relative to the oxygen atom. In both ligands, rotation of the group bound in position 2 is limited, while those positioned *para* relative to oxygen reveal rotational disorder. That seems to be characteristic for the investigated series of complexes, even in L_2^5Cu, where large atomic displacement parameters for tert-Bu are observed, although no discrete model for the disorder can be formulated. The only exception is L_3^2Cu in which such disorder does not occur. In $L_2'^1Cu$ the C36–H36A...π interaction is found with the 2.83 Å distance of C–H to the center of gravity of C1–C6 phenolic ring related by the $[x,1/2-y,-1/2+z]$ transformation.

For all structures reported here, the coordination sphere geometry is square-planar in all investigated structures and the *trans* arrangement of donor atom is found. The search in the CSD database [32] revealed that for complexes formed with the similar ligands, most of them has the *trans* architecture of the CuN_2O_2 coordination sphere. The only exception is that of bis((2-(2′-(4′,6′-di-t-butyl)phenoxy))-4,5-diphenylimidazole-N,O)-copper(ii) reported by Benisvy et al. [33]. In that structure the steric demands of the imidazole moiety seems to result in the *cis* arrangement of the ligands.

In the structures reported here, the Cu–O bonds formed by the phenolic oxygen atoms range between 1.870(3) and 1.9026(18) Å, and are shorter than those formed by the nitrogen atoms 1.9442(19) and 1.9999(12) Å. That might be attributed to the electrostatic character of the interaction between negatively charged phenolate O and central Cu(II).

In our research, the mirror plane symmetry of the L_2^1Cu complex molecule enforces the lack of displacement of atoms from the coordination plane. The O–Cu–O and N–Cu–N angles within the copper coordination sphere are 179.44(14) and179.35(15)°, respectively. The intra-ligand N–Cu–O angles [91.80(15) and 91.89(15)°] are significantly larger that the inter-ligand angles of 88.75(15) and 87.55(15)°. This effect might be explained by the larger influence of relative rigidity of the phenolate-imine moiety compared to the steric effect of N-Met moiety in the ligand.

Due to the centrosymmetric architecture of complexes L_3^2Cu and L_2^6Cu, only a small deformation of the coordination sphere is found, with the O–Cu–O and N–Cu–N angles being 180.0°. The intra-ligand N–Cu–O angles in these complexes are 91.68(5) and 91.79(12) L_3^2Cu and L_2^6Cu, respectively, and are slightly larger than the inter-ligand N–Cu–O angles of 88.32(5) and 88.22(12)°. This is analogous to the difference revealed by the L_2^1Cu structure.

Contrary to the above structures, the L_2^5Cu and $L_2'^1Cu$ complexes reveal significant deviations of the coordination sphere from the square planar CuN_2O_2. In the $L_2'^1Cu$ structure the significant steric repulsion between N-methyl and tert-Bu substituent in position 2 of the phenolate ring causes the deformation of the Cu coordination sphere, with the N–Cu–N and O–Cu–O angles being 158.73(9) and 156.97(8)°, respectively. Also the dihedral angle between the best planes of two chelate rings is 40.29(7)°. The intra-ligand O–Cu–N angles of 92.00(8) and 93.20(8)° are larger than the inter-ligand angles being 92.05(8) and 91.19(7)°.

In L_2^5Cu the bulk of phenyl-OMe bound to imine N results in the values of O–Cu–O and N–Cu–N angles far from the expected 180°, and being 143.95(6) and 139.69(6)°, respectively. The dihedral angle between best planes of two chelate rings is 53.38(4)°, and that is the largest deformation in the investigated series. Opposite to all other reported complexes, the intra-ligand O–Cu–N angles are 94.40(6) and 95.72(6)°, while the inter-ligand angles are slightly larger, being 98.11(6) and 96.22(6)°. The largest deviation of the coordination sphere from planarity and the difference in relation between the intra- and inter-ligand O–Cu–N angles strongly indicate the effect of the bulky naphthyl moiety affecting the intramolecular geometry.

3.2. Magnetic susceptibility measurements

Magnetic susceptibility χ was measured in magnetic field of 1000 Oe as a function of temperature in the range 2–300 K. The measured data were corrected for the temperature independent Larmor diamagnetic susceptibility obtained from Pascal's tables [34] and for sample holder contribution. Typical magnetic diagram is presented in Fig. 6 in the form of χ and a product χ^*T (inset) vs. T. The variation of the susceptibility χ vs. T for $T > 50$ K can be well fitted by a Curie–Weiss law. The obtained Curie constants were around 0.4 emu K/mol (0.39 emu K/mol < C < 0.42 emu K/mol) and Curie–Weiss temperatures $-1.3\ \text{K} \le \theta \le +0.12\ \text{K}$. The effective magnetic moments (μ_{eff}) calculated from the Curie constants are in the range 1.77–1.83 μ_B for all complexes indicating one unpaired electron on the copper center in the monomer complexes ($S_{Cu} = 1/2$). These values are very close to the spin only value of 1.73 μ_B [35–37] what is expected for the copper centers separated by large distances (>5 Å). Small values of Curie–Weiss temperatures θ and slight downturn of χ^*T (T) below 20 K indicate only a very weak interaction between the cooper monomers.

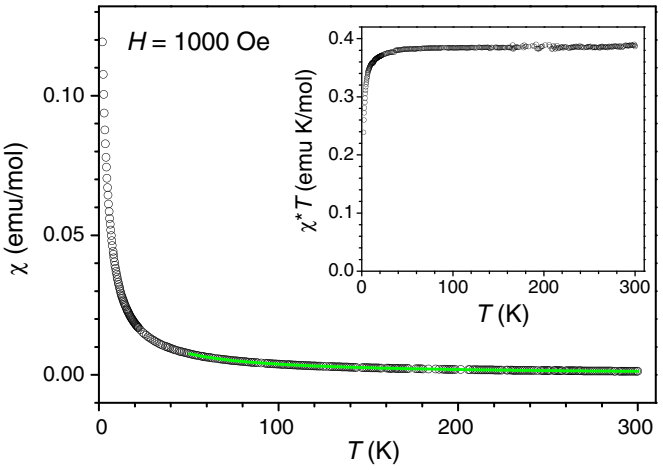

Fig. 6. Temperature dependence of magnetic susceptibility χ and a product of χ^*T (inset) as a function of temperature for the sample L_2^5Cu measured in magnetic field of 1000 Oe. The full line is a fit with a Curie–Weiss law. For all other samples (except L_2^1Cu) very similar temperature dependencies were obtained.

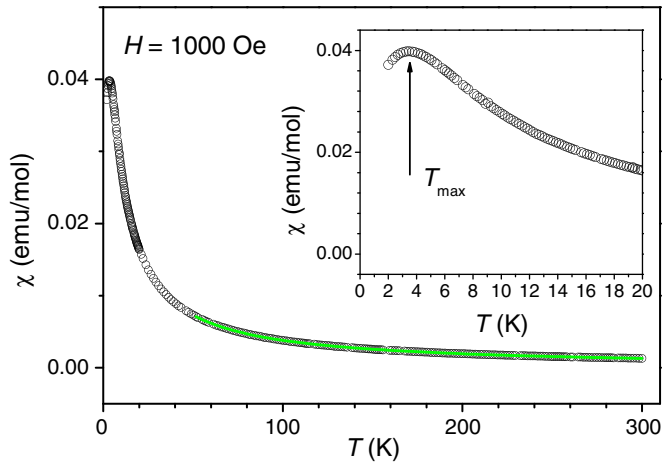

Fig. 7. Temperature dependence of magnetic susceptibility χ as a function of temperature for the sample L_2^1Cu measured in magnetic field of 1000 Oe. The full line is a fit with a Curie–Weiss law. Inset shows the position of the maximum of susceptibility in an extended temperature scale.

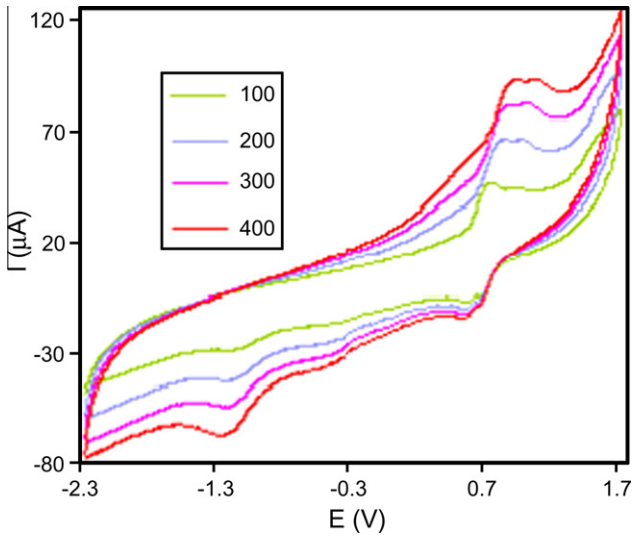

Fig. 8. Cyclic voltammogramms of L'_2Cu at −40 °C and scan rates of 100, 200, 300 and 400 mV/s.

The only exception from pure paramagnetic behavior is the sample L_2^1Cu. The magnetic susceptibility χ increases with decreasing temperature for $T > 50$ K as in the other samples (Fig. 7). However it exhibits a well pronounced cusp at a $T_{max} = 3.5$ K with a maximal value of $\chi_{max} \approx 0.04$ emu/mol. The observed temperature-dependent magnetic susceptibility demonstrates an antiferromagnetic coupling between copper centers of neighbor complexes. This is consistent with the smaller Cu1…Cu1[x,1/2−y,−z] distance of 3.3405(7) Å found in the crystal structure reported here. The Curie constant C for high temperature region ($T > 50$ K) is 0.39 ($\mu_{eff} = 1.77\ \mu_B$) as in the other samples. However, the Curie–Weiss temperature $\theta = -3.9$ K is larger compared to other samples. X-ray crystallography of this complex shows a layered structure in which copper centers are separated by a distances of around 3 Å, that favors an antiferromagnetic interaction. The coupling constant J between Cu^{2+} ions was estimated from the position of the T_{max} using the relation: $T_{max}/(|J|\cdot S\cdot(S+1)) = 2.495$ which valid for antiferromagnetic square planar lattice. For Cu^{2+} ions $S = 1/2$ and the obtained coupling constant $J = -1.3$ cm^{-1}[38].

3.3. Electrochemistry

Cyclic, square wave and differential pulse voltammograms (CV, SQW and DPV) of complexes L_2Cu and L'_2Cu have been recorded in CH_2Cl_2 solutions containing 0.1 M $[(n\text{Bu})_4\text{N}]ClO_4$ or $LiClO_4$ as supporting electrolyte. Prior to the measurement, the GC electrode was polished with 0.1 mm alumina powder and washed with distilled water. The voltage scan rate was set at 50 mV s^{-1}. The solutions were deoxygenated by bubbling nitrogen gas through them. Ferrocene was added as an internal standard after completion of a set of experiments, and potentials are referenced versus the ferrocenium/ ferrocene couple (Fc^+/Fc).

The CV voltammograms (Fig. 8) observed for all complexes revealed two oxidations (E_1^{ox} and E_2^{ox}) except for L_2^1Cu which exhibits one oxidation. Selected results are collected in Table 3. Typical cyclic voltammograms (CV) of L'_2Cu^1 are presented in Fig. 8.

E_1^{ox} and E_2^{ox} are nearly similar for mentioned complexes, what suggests that the oxidation mechanism might be the same for all complexes. These redox processes were assigned to the ligand-centered oxidation yielding the phenoxyl radical in the complex. The second oxidation potential (E_2^{ox}) are most probably arising from the oxidation of second phenolate moiety of this complexes, but there is no direct evidence for this interpretation. It is worth noting that the second oxidation potential of these complexes are more positive than that for the first ones probably due to the harder oxidation of radical cation complexes producing biradical ones.

Table 3
Electrode potentials (in V) for oxidation and reduction of copper complexes measured at −40 °C in CH_2Cl_2 solutions and referenced vs. the Fc^+/Fc couple.

Complexes	E_1[a]/V vs. (Fc^+/Fc)	E_2[a]/V vs. (Fc^+/Fc)
L_2^1Cu	0.95	
L_2^2Cu	0.84	1.19
L_3^2Cu	1.04	1.29
L_2^4Cu	0.68	1.58
L_2^5Cu	0.71	1.48
L_2^6Cu	0.67	1.32
$L_2'^1Cu$	0.67	1.1
$L_2'^2Cu$	0.98	1.22

[a] Irreversible reaction, peak potential is given.

These ligand-centered voltammograms are electrochemically irreversible, what is seen from the high separation of the peaks of reduction and re-oxidation ($\Delta E_p = Ep_a - Ep_c$). In addition, the current relationship (ip_a/ip_c) is less than unity in each case.

Comparing the oxidation potentials of mono and di-tert-butylated N-alkyl-salicylaldiminato copper complexes (L_2Cu and L'_2Cu) suggesting that anodic oxidation processes are less sensitive to the involved change in bulkiness on tert-butylated phenolic moieties of the ligands (Table 3).

On the other hand, the lower oxidation potentials of L_2^4Cu, L_2^5Cu and L_2^6Cu with aromatic groups directly attached to the imine nitrogens are probably associated with the sensitivity of anodic oxidation potentials to the involved change in mentioned groups.

The metal-centered voltammograms have been observed in the negative potential range, what corresponds to the Cu^{II}/Cu^{I} reduction of L_2Cu and L'_2Cu. They are chemically irreversible what suggests the instability of the reduced species.

4. Conclusion

We have prepared and characterized Cu(II) complexes containing bulky salicylaldimine ligands. The X-ray crystallography analysis shows that all complexes are monomer and their copper(II) centers have been surrounded by phenolate oxygens and

imine nitrogen atoms. Therefore, the coordination sphere around the copper atoms is N_2O_2 as seen in galactose oxidase active site. In addition, the geometry around the metal ion of all complexes are square planar or slightly distorted square planar with the *trans* arrangement. The crystal systems of most reported complexes are monoclinic, except L_2^1Cu for which the orthorhombic crystal system was detected.

Oxidation of the Cu(II) complexes yielded the corresponding Cu(II)- phenoxyl radical species during the cyclic voltammetry experiments. The steric and electronic effects of substituent connected to phenol and imine groups on oxidation potential have been investigated.

The observed temperature dependent magnetic susceptibility (χ) for L_2^1Cu was consistent with antiferromagnetic coupling between copper centers of neighbor complexes. The effective magnetic moment (μ_{eff}) for all other complexes are lie in the range 1.77–1.83 μ_B, indicative of an unpaired electron on copper center in monomer complexes($S_{Cu} = 1/2$). The effects of the structural factors of bulky tBu groups contributing to the effective magnetic moment have been described.

Acknowledgments

The Authors are grateful to the Institute for Advanced Studies in Basic Sciences (IASBS) Nicolaus Copernicus University, University of Ljubljana, and Changwon National University, for their valuable helps. E. Safaei gratefully acknowledges support by the Institute for Advanced Studies in 514 Basic Sciences (IASBS) Research Council under Grant No. G2010IASBS127.

Appendix A. Supplementary material

Supplementary data CCDC, 784748, 784749, 784750, 784751, and 784752 contain the supplementary crystallographic data for $L_1{}^2Cu$, $L_3{}^2Cu$, $L_5{}^2Cu$, $L_6{}^2Cu$ and $L_1{}'^2Cu$, respectively. These data can be obtained free of charge from The Cambridge Crystallographic Data Centre via http://www.ccdc.cam.ac.uk/data_request/cif. Supplementary data associated with this article can be found, in the online version, at doi:10.1016/j.ica.2010.11.017.

References

[1] R.H. Holm, P. Kennepohl, E. Solomon, Chem. Rev. 96 (1996) 2239.
[2] H.C. Liang, M. Dahan, K.D. Karlin, Science 3 (1999) 168.
[3] J. Stubbe, W.A. van der Donk, Chem. Rev. 98 (1998) 705.
[4] J. Stubbe, Chem. Commun. (2003) 2511.
[5] J.W. Whittaker, Chem. Rev. 103 (2003) 2347.
[6] R. Banerjee, Chem. Rev. 103 (2003) 2081.
[7] H. Sigel, A. Sigel, Metal Ions in Biological Systems, vol. 30, Marcel Dekker, New York, 1994. pp. 315–403.
[8] N. Ito, S.E.V. Phillips, C. Stevens, Z.B. Ogel, M.J. McPherson, J.N. Keen, K.D.S. Yadav, P.F. Knowles, Nature 350 (1991) 87.
[9] M.J. McPherson, M.R. Parsons, R.K. Spooner, C.M. Wilmot, Galactose oxidase, in: K. Wieghart, T.L. Poulos, R. Huber, A. Messerschmidt (Eds.), Handbook of Metalloproteins, vol. 2, Wiley, New York, 2001, pp. 1245–1257.
[10] M.M. Whittaker, J.W. Whittaker, Biophys. J. 64 (1993) 762.
[11] J.P. Klinman, Chem. Rev. 96 (1996) 2541.
[12] J.W. Whittaker, in: K.D. Karlin, Z. Tyeklar (Eds.), Bioinorganic Chemistry of Copper, Chapman Hall, New York, 1993, pp. 447–458.
[13] M.M. Whittaker, P.J. Kersten, N. Nakamura, J. Sanders-Loehr, E.S. Schweizer, J.W. Whittaker, J. Biol. Chem. 271 (1996) 681.
[14] M.M. Whittaker, V.L. DeVito, S.A. Asher, J.W. Whittaker, J. Biol. Chem. 264 (1989) 7104.
[15] P.F. Knowles, N. Ito, in: R.W. Hay, J.R. Dilworth, K.B. Nolan (Eds.), Perspectives in Bio-inorganic Chemistry, vol. 2, Jai, London, 1994.
[16] Y.K. Lee, M.M. Whittaker, J.W. Whittaker, Biochemistry 47 (2008) 6637.
[17] N. Ito, S.E.V. Phillips, K.D.S. Yadav, P.F. Knowles, J. Mol. Biol. 238 (1994) 794.
[18] R.M. Wachter, M.P. Montague-Smith, B.P. Branchaud, J. Am. Chem. Soc. 119 (1997) 7743.
[19] B.P. Branchaud, M.P. Montague-Smith, D.J. Kosman, F.R. McLaren, J. Am. Chem. Soc. 115 (1993) 798.
[20] R.M. Wachter, B.P. Branchaud, J. Am. Chem. Soc. 118 (1996) 2782.
[21] M.M. Whittaker, J.W. Whittaker, J. Am. Chem. Soc. 114 (1992) 3727.
[22] Brian A. Jazdzewski, William B. Tolman, Coord. Chem. Rev. 200-202 (2000) 633.
[23] A.L. Philibert, F. Thomas, C. Philouze, S. Hamman, E. Saint-Aman, J.L. Pierre, Chem. Eur. J. 9 (2003) 3803.
[24] P. Chaudhuri, M. Hess, U. Flörke, K. Wieghardt, Angew. Chem., Int. Ed. 37 (1998) 2217.
[25] Y. Wang, J.L. DuBois, B. Hedman, K.O. Hodgson, T.D.P. Stack, Science 279 (1998) 537.
[26] S. Itoh, M. Taki, S. Fukuzumi, Coord. Chem. Rev. 198 (2000) 3.
[27] F. Michel, F. Thomas, S. Hamman, C. Philouze, E. Saint-Aman, J.L. Pierre, Eur. J. Inorg. Chem. (2006) 3684.
[28] J.F. Larrow, E.N. Jacobsen, Y. Gao, Y. Hong, X. Nie, C.M. Zepp, J. Org. Chem. 59 (1994) 1939.
[29] I. Sylvestre, J. Wolowska, C.A. Kilner, E.J. McInnes, M.A. Halcrow, Dalton Trans. 19 (2005) 3241.
[30] G.M. Sheldrick, SHELXS97 and SHELXL97, University of Gőttingen, Germany, 1997.
[31] CrysAlis CCD171 and RED171 Package of Programs, Oxford Diffraction, 2000.
[32] F.H. Allen, Acta Cryst. B58 (2002) 380.
[33] L. Benisvy, A.J. Blake, D. Collison, E.S. Davies, C.D. Garner, E.J.L. McInnes, J. Mc Master, G. Whittaker, C. Wilson, Dalton Trans. (2003) 1975.
[34] R.L. Dutta, A. Syamal, Elements of Magnetochemistry, Affiliated East-West Press PVT Ltd., 1993. p. 8.
[35] L. Sacconi, Coord. Chem. Rev. 1 (1966) 126.
[36] L. Sacconi, M. Ciampolini, J. Chem. Soc. (1964) 276.
[37] B.J. Hathaway, A.A.G. Tomlinson, Coord. Chem. Rev. 5 (1970) 1.
[38] L.J. De Jongh, Magnetic Properties of Layered Transition Metal Compounds, Kluwer Academic Publishers, 1990. p. 143.